Modelling of electrochemistry and mass transport in Polymer Electrolyte Membrane Fuel Cells, PEMFC

G. Murgia, L. Pisani, M. Valentini and B. D'Aguanno*
Center for Advanced Studies,
Research and Development in Sardinia
Uta (CA), Italy

(Dated: April 19, 2001)

In this paper we present a modified version of the well know model of Bernardi and Verbrugge [1, 2] which was developed to simulate the behavior of Polymer Electrolyte Fuel Cells. The modified version is based on a different treatment of the electrokinetic model equations, the Butler-Volmer equations. Such equations are analytically integrated in the reactive regions of the electrodes, eliminating the main non-linear terms in the full mathematical model. It is shown that the modified Bernardi-Verbrugge is as accurate as the original model, that it allows an extension of the cell current density over which it is possible to find solutions, that the full numerical procedure is very stable, and that the simulations are up to three order of magnitude faster than those performed with the original model.

PACS numbers: 86.30G Fuel cells

I. INTRODUCTION

The mathematical modelling and the numerical simulation of Polymer Electrolyte Membrane Fuel Cells (PEMFC) is receiving, in these last years, more and more attention. Pioneering works can be considered those of Bernardi and Verbrugge [1, 2], and those of Springer et al. [3, 4], which made a jump from an empirical approach to a more phenomenological and mechanistic type of approach. In these works, the membrane electrode assembly (MEA) was divided into several regions, and for each region equations for the charge and mass transport were written down. The description of the MEA was kept at the one-dimensional level, mainly because the essential features of the performance curve of a MEA (cell potential versus cell current density) are already well described at this level, while the computational complexity is still affordable.

Since then, most of the successive work followed two main streams. In one case, effort has been paid to go from the 1D modelling to 2D, and even 3D, modelling. These higher dimensionality models offer the possibility to describe the hydrodynamics and multi-component transport inside the flow channel for reactant distribution (see Fig. 1 of the next section), and to take into account different geometries, or flow field configurations, of the flow channels. Clear prototype works of 2D modelling and simulation have been made by Gurau, Liu and Kakac [5], by Kulikovsky et al. [6] and by Um, Wang and Chen [7]. A 3D modelling has been developed by Divisek et al. [8] but unfortunately no implementation of the model has been performed.

In the other work stream, attention has been devoted to the inclusion into the models of a more extended phenomenology, such as heat transport, proton transport in membrane with variable water content, membrane permeability, electrode flooding, transient phenomena, etc. (for reviews on the state of the art see Gottesfeld, Zawodzinski [9] and Gurau [10]). However, the approaches developed in these works are, very often, only devoted to partial aspects, loosing the ability to construct global models.

In this work we reviewed critically the 1D model of Bernardi and Verbrugge [1, 2] (BV model), and we developed a modified version of such a model, the modified BV model (MBV), with the aim to establish a numerically stable and fast 1D model, which will be able to act as a starting point for 2D and 3D generalizations, as well as a starting point for the inclusion of energy transport, water management and transient phenomena.

To establish a numerical stable and fast model we modified the treatment of the electrochemical kinetic, both at the cathode and at the anode. The modification is based on the observation that, already from a very small cell current density on, the reactants are quantitatively consumed in a very thin region at the interface between the diffusive and reactive regions of the electrodes. On the base of this observation, it is possible to analytically integrate the equations describing the electrochemical kinetic, the Butler-Volmer equations, eliminating, in this way, the highly non-linear part of the mathematical modelling. The resulting integrated equations are then inserted in a BV-like scheme, which is essentially based on conservative and constitutive equations for the mass and charge transport. The MBV scheme is closed with the appropriate boundary conditions, and a solution algorithm is constructed by using the finite volume method.

The paper is organized as follows. In the modelling section we review the basic assumptions and equations of the BV model, we describe the integration of the Butler-Volmer equations, and we report, as a table, the full set of equations for both the BV and MBV models. The two

*Electronic address: bruno@crs4.it

models are contrasted and discussed at length. In the section devoted to the results, the computational advantages of the MBV model over the BV model are presented, together with comparisons showing that the accuracy of the two models is the same. We stress the point that the numerical simulations performed with the MBV model are up to three order of magnitude faster than those based on the BV model. The paper is ended with the conclusions, where future applications of the model are presented.

II. MODELLING

A. Review of the BV model

1 Model regions

As it is becoming usual in 1D analytical approaches to the modelling of PEMFC, the unit cell is divided into seven regions [11], three for the anode compartment, A, one for the electrolyte, M, and three for the cathode compartment, C. By going from the anode to the cathode side, we have (see Fig. 1): (I) the anode flow region, A_F; (II) the anode diffusion region, A_D; (III) the anode reaction region, A_R; (IV) the ion transport region, or membrane, M; (V) the cathode reaction region, C_R; (VI) the cathode diffusion region, C_D; (VII) the cathode flow region, C_F. For the boundaries between the various regions we will use the notation A_F/A_D, A_D/A_R, etc. In the BV model the zero of all position dependent variables is set at the A_D/A_R boundary, and the distance z grows in the direction from the anode to the cathode.

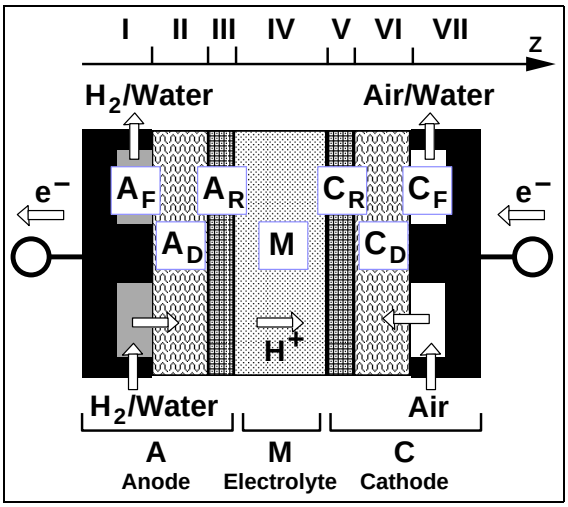

FIG. 1: The seven regions of a PEMFC 1D model

This division of the unit cell is motivated by the fact that in each of the mentioned region different chemical and physical transport phenomena occur. In addition, different regions are made of different materials.

The flow regions correspond to the channels dug into the bipolar plates, and they are used to distribute hydrogen (the A_F region), and air or oxygen (the C_F region). Once the reactant gases get into contact with the regions A_D and C_D, they diffuse through them reaching the reaction regions A_R and C_R. In A_R, hydrogen is catalytically oxidized with the release of electrons and H^+ ions. The electrons move through the solid electronic conducting part of the A_R, A_D and bipolar plate regions reaching, in this way, the external circuit. The H^+ ions take the opposite direction and they move into the membrane region, M, by reaching the cathode reaction region, C_R. Here they get into contact with the oxygen molecules and the electrons. The contact is happening on the surface of the catalyst present in the region, where the species react by releasing water heat. To reach the catalyst surface, oxygen molecules had to come from the regions C_F and C_D. The same regions are crossed by the electrons coming from the external circuit, although the transport occurs, as already said, through the solid electronic conducting part of the regions.

However, in the BV model not all regions are treated in the same way. A numerical approach is used to solve the model equations of regions III, IV, V and VI, while those of regions I, II and VII are solved analytically.

2 Model variables, assumptions and conservation laws

The independent variables taken into account by the model are the electrical potential of the solid and liquid phases, respectively Φ_s and Φ, the hydraulic pressure, P, the oxygen and hydrogen concentrations, c_{O_2} and c_{H_2}, and the concentration of nitrogen, x_{N_2}, expressed as molar fraction of N_2 over the total molar concentration at the cathode.

It is well known that the spatial variations of such variables can act as driving forces for mass and charge flux, that the approximated equations expressing the relation between flux and driving forces are the constitutive equations, and that flux follow conservation equations. Therefore, the closed set of model equations is derived by combining together the constitutive and conservation equations of the electric current, both electronic $\mathbf{i}_s$ and ionic $\mathbf{i}$, and of the mass flux $\mathbf{N}_i$, with $i = H_2, O_2, N_2, H_2O$. All independent variables and related flux are functions of position z but to keep the notation simple such a dependence will be omitted. Instead, the vectorial notation, although not strictly necessary, will be kept.

A summary of all described variables, transport phenomena and conservation equations is given in Table I, where these quantities are grouped according to the FC regions of Fig. 1. The terms j^A, j^C and y_i are the current and mass source terms, respectively, and they are due to the anode and cathode electrochemical reactions. The term $\mathbf{v}$ is the velocity of liquid water in the pores, which is directly linked, as we will see in the next section, to the hydraulic pressure. The lower index w stays for liquid water.

TABLE I: The modelled transport phenomena and the conservation equations

Regions	Variables	Flux	Conservation
A_D	c_{H_2}, Φ_s, P	$\mathbf{N}_{H_2}, \mathbf{i}_s, \mathbf{v}$	$\nabla\cdot\mathbf{N}_{H_2} = \nabla\cdot\mathbf{i}_s = \nabla\cdot\mathbf{v} = 0$
A_R	c_{H_2}, Φ_s, Φ, P	$\mathbf{N}_{H_2}, \mathbf{i}_s, \mathbf{i}, \mathbf{v}$	$\nabla\cdot\mathbf{N}_{H_2} = y_{H_2}$, $\nabla\cdot\mathbf{i}_s = -\nabla\cdot\mathbf{i} = j^A, \nabla\cdot\mathbf{v} = 0$
M	$c_{H_2}, c_{O_2}, \Phi, P$	$\mathbf{N}_{H_2}, \mathbf{N}_{O_2}, \mathbf{i}, \mathbf{v}$	$\nabla\cdot\mathbf{N}_{H_2} = \nabla\cdot\mathbf{N}_{O_2} = \nabla\cdot\mathbf{i} = \nabla\cdot\mathbf{v} = 0$
C_R	c_{O_2}, Φ_s, Φ, P	$\mathbf{N}_{O_2}, \mathbf{i}_s, \mathbf{i}, \mathbf{v}$	$\nabla\cdot\mathbf{N}_{O_2} = y_{O_2}$, $\nabla\cdot\mathbf{i}_s = -\nabla\cdot\mathbf{i} = j^C, \nabla\cdot\mathbf{v} = \rho y_w$
C_D	$c_{O_2}, x_{N_2}, \Phi_s, P$	$\mathbf{N}_{O_2}, \mathbf{N}_{N_2}, \mathbf{i}_s, \mathbf{v}$	$\nabla\cdot\mathbf{N}_{O_2} = \nabla\cdot\mathbf{N}_{N_2} = \nabla\cdot\mathbf{i}_s = 0$, $\nabla\cdot\mathbf{v} \propto \nabla\cdot\mathbf{N}_w$

We can observe that time and temperature are not included in the description and, therefore, the model does not take into account transient phenomena and heat flux. The cell temperature is assumed to be constant, and all inlet gases are assumed to instantaneously equilibrate with such temperature. Other model assumptions are (see ref. [2] for an extended presentation): *(i)* in the regions A_D and C_D, gases are transported through hydrophobic pores, while liquids through hydrophilic pores; *(ii)* the gas pressure in the regions A_D and C_D is constant and equal to the inlet pressure; *(iii)* the inlet gases are water saturated; *(iv)* the membrane is always fully hydrated.

3 Charge and mass transport: constitutive laws

In the membrane, M, and in the reaction regions, A_R and C_R, the neutral chemical species flux is due to diffusion and convection and it is described by

$$\mathbf{N}_i = -D_i\nabla c_i + c_i\mathbf{v} \quad \text{for} \begin{cases} i = H_2 & \text{in } A_R \\ i = H_2, O_2 & \text{in M} \\ i = O_2 & \text{in } C_R \end{cases} , \quad (1)$$

which is the Nernst-Planck equation [11]

$$\mathbf{N}_i = z_i\beta_F D_i c_i \nabla\Phi - D_i\nabla c_i + c_i\mathbf{v} \quad , \quad (2)$$

without the migration term. Here z_i is the charge number of species i, D_i its diffusion coefficient, $\beta_F = F/RT$ is the Faraday constant, F, in units of RT, with R the gas constant.

In the porous regions A_D and C_D it is assumed that the motion of gases is separated from that of liquids. For the diffusive motion of a gas of species i and molar fraction x_i in an ideal gas mixture we use the Stefan-Maxwell equation [12]

$$\nabla x_i = \sum_{j=1}^{n} \frac{RT}{PD_{ij}}(x_i\mathbf{N}_j - x_j\mathbf{N}_i) \quad \text{for} \begin{cases} i = O_2, N_2, wH_2O & \text{in } C_D \\ i = H_2, H_2O & \text{in } A_D \end{cases} , \quad (3)$$

in which D_{ij} is the ij-pair diffusion coefficient in a binary mixture.

The concentration of the liquid species in equilibrium with the coexisting gas phase are locally obtained by using the Henry's law

$$c_i = x_i\frac{P}{K_i} \quad \text{for} \begin{cases} i = O_2, N_2, H_2O & \text{in } C_D, \\ i = H_2, H_2O & \text{in } A_D \end{cases} , \quad (4)$$

where K_i is the Henry constant.

The electronic current, $\mathbf{i_s}$ is modelled by the Ohm's law

$$\mathbf{i}_s = \sigma\nabla\Phi_s \qquad \text{in } A_D, A_R, C_R, C_D \quad , \quad (5)$$

while the ionic current, $\mathbf{i}$, is described by

$$\mathbf{i} = -\kappa\nabla\Phi + Fc_f\varepsilon\mathbf{v} \qquad \text{in } A_R, M, C_R \quad , \quad (6)$$

where σ and κ are the material dependent electronic and ionic conductivity, respectively, and ε the volume fraction of the convective fluid.

To describe the water velocity in the porous regions we use the following modified version of the Schlögl equation [13–15]

$$\mathbf{v} = \frac{k_\Phi}{\mu}z_f c_f F\nabla\Phi - \frac{k_p}{\mu}\nabla P \qquad \text{in } A_R, M, C_R \quad , \quad (7)$$

in which z_f and c_f are the valence and the concentration of the membrane charges, k_Φ and k_p are the electrokinetic and hydraulic permeabilities, and μ the pore-fluid viscosity. Such water velocity, which is the velocity in the pores, or void phase, is connected to the velocity of water flowing through a planar surface (perpendicular to $\mathbf{v}$), v_s, via the volume fraction of the water phase, ε

$$\mathbf{v}_s = \varepsilon\mathbf{v} \quad . \quad (8)$$

More specifically, for the various regions the used relations are

$$\mathbf{v}_s = \varepsilon_M^\beta\varepsilon_w^M\mathbf{v} \qquad \text{for} \quad \beta = A_R, C_R \quad (9)$$

$$\mathbf{v}_s = \varepsilon_w^M\mathbf{v} \qquad \text{in} \quad M \quad , \quad (10)$$

where ε_α^β is the volume fraction of phase α in the region β.

In the regions A_D and C_D, where ionic charges are absent, the Schlögl equation does not contain the electric potential term and reduces to the Darcy equation

$$\mathbf{v} = -\frac{k_p}{\mu}\nabla P \qquad \text{in } A_D, C_D \quad . \quad (11)$$

4 Electrochemistry: source terms

The charge and mass source terms of Table I originate from the anode and cathode electrochemical reactions

$$2H_2 \rightleftarrows 4H^+ + 4e^- \quad \text{overall in } A_R \quad (12)$$
$$H_2 \rightleftarrows 2H_{ads} \quad \text{step in } A_R \quad (13)$$
$$H_{ads} \rightleftarrows H^+ + e^- \quad \text{step in } A_R \quad (14)$$
$$O_2 + 4H^+ + 4e^- \rightleftarrows 2H_2O \quad \text{overall in } C_R \quad (15)$$

At the anode, H_2 is assumed to be adsorbed on the catalyst and then electrochemically dissociated via a one-electron step. Very roughly, O_2 is assumed to dissociate in a four-electron step.

A simple type of dependence of the current density variation on the electrode kinetic is given by the Butler-Volmer equation [11, 16]

$$\nabla \cdot \mathbf{i} = j^\beta = i_0^\beta \Big[e^{\alpha_a^\beta \beta_F (\Phi_s - \Phi)} - e^{-\alpha_c^\beta \beta_F (\Phi_s - \Phi)} \Big] \quad , \quad (16)$$

in which i_0^β is the exchange current density at the electrode of type β, and $\alpha_a^\beta, \alpha_c^\beta$ the anode and cathode transfer coefficients of the semi-redox reactions at that electrode.

The term i_0^β is related to the chemical composition close to the electrode β, and an approximate expression for it is [2, 11]

$$i_0^\beta = a i_{0,ref}^\beta \prod_i \Big(\frac{c_i}{c_{i,ref}} \Big)^{\gamma_i} \quad , \quad (17)$$

where a is the reaction area per unit volume, $i_{0,ref}^\beta$ the exchange current density for the reference compositions $c_{i,ref}$, c_i the local concentrations, and γ_i the exponents which can be linked to the stoichiometric coefficients of the rate determining step.

At the same time, mass variations also occur and they are proportional to the current density variations given in the previous eqns (16) and (17). The relation is

$$y_i = \frac{s_i^\beta}{n^\beta F} j^\beta \qquad \text{for} \begin{cases} i = H_2 & \text{in } A_R, \\ i = O_2, w & \text{in } C_R \end{cases} \quad , \quad (18)$$

where s_i^β are the stoichiometric coefficients and n^β the number of electrons involved in the electrochemical reactions.

For the particular reaction scheme given in eqs. (12)-(15), all the electrochemical parameters introduced in this Section are reported in Table II.

TABLE II: Electrochemical parameters

Quantity	Anode	Cathode
Exchanged electrons, n	1	4
H_2 stoichiometric coefficient, s_{H_2}	1/2	—
O_2 stoichiometric coefficient, s_{O_2}	—	-1
w stoichiometric coefficient, s_w	—	2
O_2 concentration exponent, γ_{O_2}	—	1/2
H_2 concentration exponent, γ_{H_2}	1/4	—
H^+ concentration exponent, γ_{H^+}	1/2	2

B. Modified version of the BV model, MBV

The BV model reviewed in the previous sections has many drawbacks. Such drawbacks are mainly connected with the chemical physics assumption of section II A 2 and, to a certain extension, with the interplay between the derived equation set, the chosen solution method and algorithm, and the requested values for the input parameters. While the chemical physics assumptions are critical for the ability of the model to describe and predict, both quantitatively and qualitatively, the experimental outcomes, the computational aspects are critical for the practical finding of solutions. From "a posteriori" view point, it turns out that the range of input parameters which require very long iteration runs, and for which numerical instabilities are found, is quite large, and often involves parameter regions of practical interest.

The appearance of numerical problems can be mainly traced back to the nonlinearity introduced by the Butler-Volmer eqs. (16), (17), and to the very steep gradients of H_2 and O_2 concentrations in the reactive regions A_R and C_R. In addition, the H_2 and O_2 concentrations go to zero very abruptly with a slope different from zero adding more numerical problems.

On the other hand, the more steep is the gradient concentration the less thick is the extent of the regions A_R and C_R in which the concentration of H_2 and O_2 is significantly different from zero, and already for very small current densities, the bulk redox reactions of eqs. (12) and (15) become surface reactions, occurring at the interfaces A_D/A_R and C_D/C_R, respectively.

To put the BV model on a more stable numerical ground while keeping the essential modelling features (or, in other words, while keeping the same degree of numerical accuracy), *the BV model has been modified by adding the assumption that, from a very low current density on (to be specified), the anode and cathode reactions are only taking place at the A_D/A_R and C_D/C_R interfaces, respectively.*

As a consequence of such a modification, *in the regions A_R and C_R the modified BV model only describes the flux of ionic charge and water, which still have to be solved explicitly (see Table I for comparison), puts all source terms equal to zero, and the anode and cathode electrochemistry survives as boundary condition at the A_D/A_R and C_D/C_R interfaces*

C. The complete equation set

The conservation equations of Table I, the constitutive equations, eqs. (2)-(11), and the source term relations (16)-(18) can be easily manipulated to yield the complete set of coupled elliptic equations to be solved.

Table III reports such equations for both the BV and MBV models. Since the MBV model has no source terms in the A_R and C_R regions , it appears to be more simple then the BV model.

TABLE III: Full system of coupled elliptic equations

Variables	Equations		Validity regions
c_{H_2}	$\nabla\cdot\left(D^*_{\mathrm{H}_2}\nabla c_{\mathrm{H}_2} - c_{\mathrm{H}_2}\mathbf{v}\right)=0$		M
	$= y_{\mathrm{H}_2}$	for the BV model	$\mathrm{A_R}$
	$=0$	for the MBV model	$\mathrm{A_R}$
c_{O_2}	$\nabla\cdot\left(D^*_{\mathrm{O}_2}\nabla c_{\mathrm{O}_2} - c_{\mathrm{O}_2}\mathbf{v}\right)=0$		M
	$= y_{\mathrm{O}_2} - \frac{c_{\mathrm{O}_2}}{\rho}y_w$	for the BV model	$\mathrm{C_R}$
	$=0$	for the MBV model	$\mathrm{C_R}$
x_{N_2}	$\frac{P_{inlet}}{RT}\frac{D^*_{w-\mathrm{N}_2}}{x_{\mathrm{N}_2}}\nabla x_{\mathrm{N}_2} = \frac{\mathbf{I}}{n^C F}r_{\mathrm{N}_2} + \mathbf{N}_w$		$\mathrm{C_D}$
Φ_s	$\nabla\cdot\left(\sigma\nabla\Phi_s\right)=0$		$\mathrm{A_D}$, $\mathrm{C_D}$
	$= j^A$	for the BV model	$\mathrm{A_R}$
	$= j^C$	for the BV model	$\mathrm{C_R}$
	$=0$	for the MBV model	$\mathrm{A_R}$, $\mathrm{C_R}$
Φ	$\nabla\cdot\left(-\kappa\nabla\Phi + Fc_f\varepsilon\mathbf{v}\right)=0$		M
	$\nabla\cdot\left(-\kappa^*\nabla\Phi\right)= j^A$	for the BV model	$\mathrm{A_R}$
	$= j^C - \frac{Fc_f}{\rho}y_w$	for the BV model	$\mathrm{C_R}$
	$=0$	for the MBV model	$\mathrm{A_R}$, $\mathrm{C_R}$
P	$\nabla\cdot\left(-\frac{k_p}{\mu}\nabla P\right)=0$		$\mathrm{A_D}$, $\mathrm{C_D}$
	$\nabla\cdot\left(b\nabla\Phi - \frac{k_p}{\mu}\nabla P\right)=0$		M
	$= -\frac{1}{\rho}y_w$	for the BV model	$\mathrm{C_R}$
	$=0$	for the MBV model	$\mathrm{A_R}$, $\mathrm{C_R}$

In this Table:
$\mathbf{I} = \mathbf{i}_s - \mathbf{i}$; $b = \frac{k_\phi}{\mu}z_f c_f F$; $r_{\mathrm{N}_2} = D^*_{w-\mathrm{N}_2}/D^*_{\mathrm{N}_2-\mathrm{O}_2}$; $r_w = D^*_{w-\mathrm{N}_2}/D^*_{w-\mathrm{O}_2}$; $\mathbf{N}_w = \mathbf{I}/(n^C F)x_w^{sat}(x_{\mathrm{O}_2} + x_{\mathrm{N}_2}/r_w)^{-1}$.

D. Boundary conditions

The boundary conditions for the BV model are reported in Table IV. In the Table, the subscript $-$ refers to the region on the left of the interface, while the subscript $+$ to the region on the right.

From the Table we see that the flux of dissolved hydrogen is continuous at the $\mathrm{A_R}$/M boundary, while that of dissolved oxygen is such at the M/$\mathrm{C_R}$ boundary. At the boundary $\mathrm{A_D}$/$\mathrm{A_R}$ the value of c_{H_2} is given, and such value corresponds to the inlet concentration.

TABLE IV: Boundary conditions of the BV model

	$\mathrm{A_D}$/$\mathrm{A_R}$	$\mathrm{A_R}$/M	M/$\mathrm{C_R}$	$\mathrm{C_R}$/$\mathrm{C_D}$
c_{H_2}	$c_{\mathrm{H}_2}\vert_- = (1-x_w^{sat})\frac{P_A}{K_{\mathrm{H}_2}}$	$D_{\mathrm{H}_2}\nabla c_{\mathrm{H}_2}\vert_- = D_{\mathrm{H}_2}\nabla c_{\mathrm{H}_2}\vert_+$	$c_{\mathrm{H}_2}\vert_- = 0$	$---$
c_{O_2}	$---$	$c_{\mathrm{O}_2}\vert_+ = 0$	$D_{\mathrm{O}_2}\nabla c_{\mathrm{O}_2}\vert_- = D_{\mathrm{O}_2}\nabla c_{\mathrm{O}_2}\vert_+$	$c_{\mathrm{O}_2}\vert_+ = (1-x_{\mathrm{N}_2}\vert_+ - x_w^{sat})\frac{P_C}{K_{\mathrm{O}_2}}$
$x^\dagger_{\mathrm{N}_2}$	$---$	$---$	$---$	$---$
Φ_s	$\sigma\nabla\Phi_s\vert_- = \sigma\nabla\Phi_s\vert_+$	$\sigma\nabla\Phi_s\vert_- = 0$	$\sigma\nabla\Phi_s\vert_+ = 0$	$\sigma\nabla\Phi_s\vert_- = \sigma\nabla\Phi_s\vert_+$
Φ	$\Phi_+ = 0$	$\kappa\nabla\Phi\vert_- = \kappa\nabla\Phi\vert_+$	$\kappa\nabla\Phi\vert_- = \kappa\nabla\Phi\vert_+$	$\kappa\nabla\Phi\vert_- = Fc_f\varepsilon_M^C\mathbf{v}\vert_-$
P	$\frac{\mathbf{N}_w}{\rho} - \frac{k_p}{\mu}\nabla P\vert_- = b'\nabla\Phi\vert_+ - \frac{k_p^*}{\mu}\nabla P\vert_+$	$b'\nabla\Phi\vert_- - \frac{k_p^*}{\mu}\nabla P\vert_- = b\nabla\Phi\vert_+ - \frac{k_p}{\mu}\nabla P\vert_+$	$b\nabla\Phi\vert_- - \frac{k_p}{\mu}\nabla P\vert_- = b'\nabla\Phi\vert_+ - \frac{k_p^*}{\mu}\nabla P\vert_+$	$b'\nabla\Phi\vert_- - \frac{k_p^*}{\mu}\nabla P\vert_- = \frac{\mathbf{N}_w}{\rho} - \frac{k_p}{\mu}\nabla P\vert_+$

†: the boundary condition for x_{N_2} is given at the $\mathrm{C_D}$/$\mathrm{C_F}$ interface. See text for its expression.
In this Table:
$b' = \varepsilon_{\mathrm{M}}\frac{k_\phi^*}{\mu}z_f c_f F$; $b = \frac{k_\phi}{\mu}z_f c_f F$; See Table III for other symbols.

The transport equation for x_{N_2} is a first order differen-

tial equation, and we only need to specify one boundary condition. At the C_D/C_F interface, such condition is given by the following expression [2]

$$x_{N_2} = (1 - x_w^{sat}) \frac{\zeta}{\zeta - 1} \frac{x_{N_2}^C}{x_{O_2}^C} \Big(1 + \frac{\zeta}{\zeta - 1} \frac{x_{N_2}^C}{x_{O_2}^C} \Big)^{-1} \quad , \quad (19)$$

where ζ is the stoichiometric inlet flow for O_2, $x_{N_2}^C/x_{O_2}^C$ the inlet N_2-O_2 molar ratio, and x_w^{sat} the gas-phase molar ratio of water at saturated condition.

The electronic current, $\mathbf{i}_s$, is continuous at the A_D/A_R and C_R/C_D boundaries, and the ionic current, $\mathbf{i}$, is such at A_R/M and M/C_R. While a boundary value for Φ is given and arbitrarily fixed to zero at A_D/A_R, no boundary value can be specified for Φ_s.

In the regions A_D and C_D water is present as liquid and gas. Then, the continuity of the total flux of water at the interfaces A_D/A_R and C_R/C_D is given by

$$\rho \mathbf{v}_s|_{-/+} + \mathbf{N}_{w,g} = \rho \varepsilon_M^\beta \varepsilon_w^M \mathbf{v}|_{-/+} \quad \text{for } \beta = A_R, C_R \quad , \quad (20)$$

where the left term refers to the A_D or C_D sides of the interfaces. Instead, at the A_R/M and M/C_R interfaces, water is present as liquid only, and we have the continuity in the superficial flux

$$\mathbf{v}|_{-/+} = \varepsilon_M^\beta \mathbf{v}|_{-/+} \qquad \text{for } \beta = A_R, C_R \quad . \quad (21)$$

In the modified BV model, the transformation of the bulk reactions to a surface reactions imposes new boundary conditions at the A_D/A_R and C_R/C_D interfaces. Since the boundary conditions at the other interfaces remain unchanged, Table V only reports the new conditions.

TABLE V: Boundary conditions of the modified BV model

	A_D/A_R	C_R/C_D
Φ_s	$\sigma \nabla \Phi_s\|_- = \sigma \nabla \Phi_s\|_+ \; ; \quad \Phi_s\|_+ = \Phi\|_+ + \eta^A$	$\sigma \nabla \Phi_s\|_- = \sigma \nabla \Phi_s\|_+ \; ; \quad \Phi_s\|_- = \Phi\|_- + \eta^C$
P		$b^* \nabla \Phi\|_- - \frac{k_p^*}{\mu} \nabla P\|_- - \frac{s_w}{n^C F \rho} I = \frac{\mathbf{N}_w}{\rho} - \frac{k_p}{\mu} \nabla P\|_+$

The extension of the discontinuities of η^A and η^C ($\eta = \Phi_s - \Phi$) at the A_D/A_R and C_R/C_D interfaces is obtained through an approximate analytical integration of the Butler-Volmer equation, eq. (16), for the anode and cathode reactions. By following the derivation reported in Appendix A, such discontinuities are given by

$$\eta^A = \frac{1}{\alpha^A \beta_F} \ln \Big(B + \sqrt{B^2 + 1} \Big) \quad , \quad (22)$$

$$\eta^C = -\frac{1}{\alpha_c^C \beta_F} \Big\{ 2 \ln I - \ln \Big(\frac{2 n^C F D_{O_2}}{s_{O_2}^C (\gamma_{O_2} + 1)} a i_{0\text{ref}}^C c_{O_{2\text{ref}}} \Big) - (\gamma_{O_2} + 1) \ln \Big(\frac{c_{O_2}^{C_D/C_R}}{c_{O_{2\text{ref}}}} \Big) \Big\} \quad , \quad (23)$$

in which

$$B = \frac{s_{H_2}^A I^2 c_{H_{2\text{ref}}}^{\gamma_{H_2}} (\gamma_{H_2} + 1)}{2 n^A F \; a \; i_{0\text{ref}}^A \Big(c_{H_2}^{A_D/A_R} \Big)^{\gamma_{H_2}+1} D_{H_2}} \quad . \quad (24)$$

At the same time, a new term is added to the left side of the continuity equation for the total flux of water at the C_R/C_D, which expresses the total amount of water produced by the cathode surface reaction

$$w_{tot} = \frac{s_w^C}{n^C F \rho} I \quad . \quad (25)$$

E. The numerical solution

From the numerical solution point of view, the BV model and the MBV model are formally treated in the same way.

The unknown spatial functions $c_{H_2}, c_{O_2}, x_{N_2}, \Phi_s, \Phi, P$, and the set of defining equations, are discretized by using the method of finite volumes. The choice of this method is based on: *(i)* the compactness of the written codes (for complex problems, too); *(ii)* its robustness and stability; *(iii)* the "low computational cost" (which is extremely important for the treatment of 2D and 3D cases); and *(iv)* last but not least, the closeness of the method to the physical reality, since it is based on the flux balance through the boundaries of the discretization cell (known as control volume). An introduction to the method and its advantages over other schemes for the specific problem we are dealing with (a system of elliptic equations) can be found in refs. [17, 18].

The discretization of the equations in the mentioned unknowns yields a nonlinear finite system in which the unknowns are the average values over the control volumes of $c_{H_2,i}, c_{O_2,i}, x_{N_2,i}, \Phi_{s,i}, \Phi_i, P_i$, with i going from

1 to the number of chosen discretization points. Moreover, and to be once more close to physics, the discretized space has been structured into domains coinciding with the model regions. To handle the boundary conditions on the domains, the Dirichelet-Neumann method has been chosen [17]. In conclusion, the equation system has been numerically solved by using the finite volume method, the Dirichelet-Neumann method for the domain boundary conditions, four domains (A_R, M, C_R, C_D), and a number of discretization points up to 7000 (which means a number of true unknown up to ≈ 25000). The solution is searched by using straightforward iteration methods. In the region A_D the system is solved analytically.

The corresponding computer code has been written in FORTRAN90 by using an object-oriented style, and it is heavily based on the construct "module", which allows an easy upgrade and maintenance of the full code. The solution kernel is made of ≈ 10000 lines of instructions. The code runs on several UNIX work-stations (IBM, HP, Silicon Graphics).

III. RESULTS

All the presented results of this paper are based on the membrane properties, and electrode parameters and properties reported in Tables II and III of the Bernardi-Verbrugge work [2]. Many of the results are also based on the physical parameters for base-case conditions reported in Table I of the same work. The reader is then addressed to such a work for the precise value of all input (apart for some miss print in the electrochemical parameters, but in this case see the correct values of Table II in this work).

As a first set of results we show, in Fig. 2, the concentration profiles of dissolved gases through the three regions A_R, M and C_R. The results are obtained by using the BV model and all parameters for the mentioned base-case. It is evident that already at very low current density ($i \approx 1 \times 10^{-2}$A/cm^2), the O_2 concentration goes to zero in the first 10% of thickness of the region C_R close to C_D, while the H_2 concentration is almost zero at the A_R/M interface. For slighter greater current densities, both concentration profiles O_2 and H_2 go abruptly to zero at the C_R/C_D and A_D/A_R interfaces, respectively.

These observation strongly motivated the development of the MBV model, and in Fig. 3 we show a comparison between the performance curves as obtained from the BV and the MBV models, always for the base-case of ref. [2]. We can observe that the MBV model gives results for a more extended current density range (once is fixed the number of grid points), that the MBV model differs from the BV model at very low current density (see figure inset), and at current densities close to the breakup in the BV model, while for intermediate current the two models are indistinguishable.

While the differences at very low current densities are due to the failure of the MBV model approximations, the differences close to the current densities of the BV model breakup are due to numerical inaccuracy of the BV model

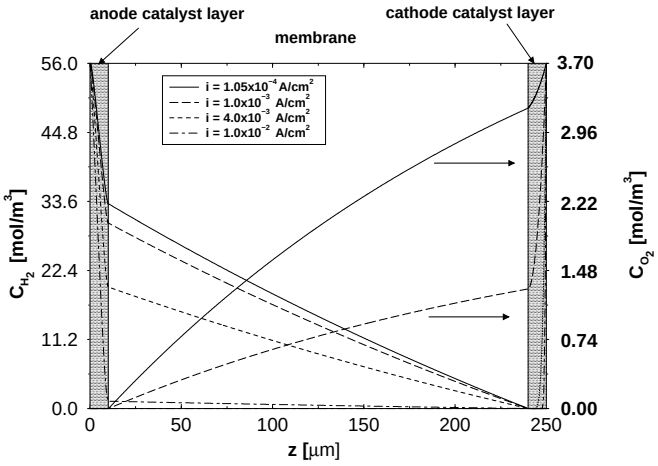

FIG. 2: Concentration profiles for H_2 and O_2. Input data and parameters refer to the base-case of ref [2]

(while the MBV model becomes more precise). These numerical inaccuracy of the BV model originate from the inability of the finite volume method to treat very steep functions with a limited number of grid points. Clearly, such inaccuracy could be eliminated by increasing the number of grid points but the price to be paid is an increasingly long, and impractical, computational time.

Figure 4 reports a comparison between the computational times of the two models for the same calculations of Fig. 3, together with computational time results from a calculation made within the BV model, by requiring the same accuracy of the MBV model, where same accuracy means indistinguishable performance curves. By comparing the results for the two cases with the same degree of accuracy (solid line and long dashed line), we can observe that at the highest current density of the current Fig. 4, the MBV model is more than two order

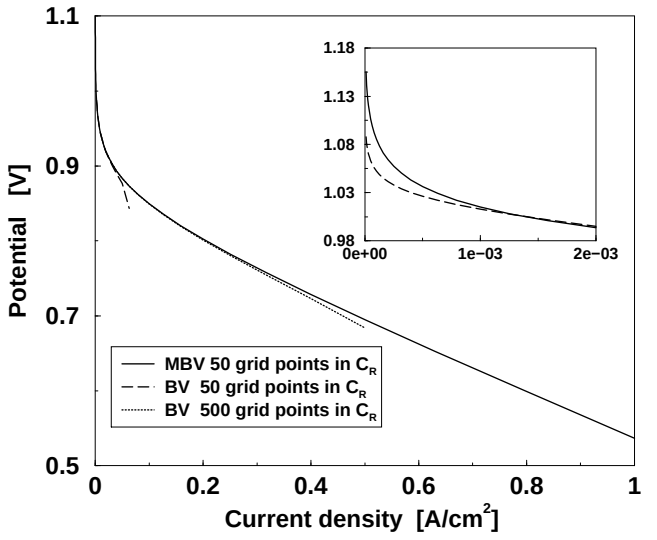

FIG. 3: Performance curves from BV and MBV models. Input data and parameters refer to the base-case of ref [2]

of magnitude faster than the BV model (cpu time for $I = 1\text{A/cm}^2$: MBV $\approx$ 20s; BV $\approx$ 4000s). On the other hand, to try to spear computational time within the BV model is useless, since the spearing can only be achieved by loosing accuracy, and by decreasing the current density range of applicability of the model.

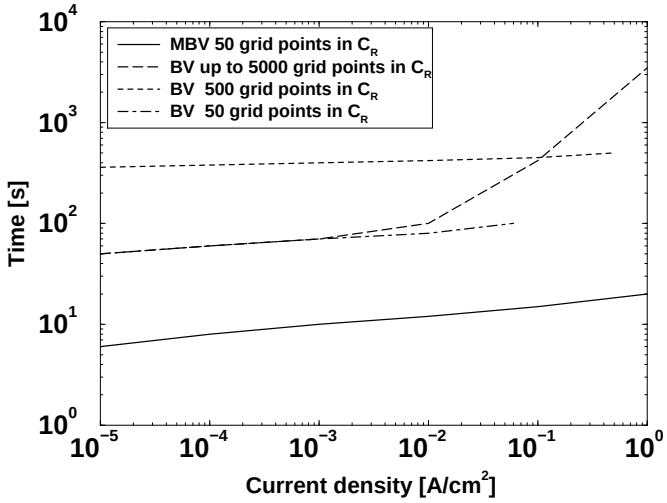

FIG. 4: Computational times to run simulations within the BV and MBV models

For sake of completeness, and to better judge the approximations used to derive the MBV model (see Appendix A), Table VI gives the relative errors of the three used approximations, where the relative error of a quantity λ is defined as

$$\text{rel.err.}(\lambda) = \left| \frac{\lambda_{BV} - \lambda_{MBV}}{\lambda_{BV}} \right| \quad . \tag{26}$$

The errors are evaluated for the performance curves with the same accuracy, with cell current density varying from 1 to 1000 mA/cm ^{2}. From this Table it is seen that errors are very small in all the considered range. Instead, and as obvious from the inset of Fig 3, notable effects of the approximations are evident for very small cell currents ($I < 1mA/cm^3$).

TABLE VI: Relative errors of the MBV model

Approximation	Relative error
$\nabla(\phi_{sol} - \phi) = 0$	$< 10^{-3}$
$c_k v = 0$	$< 10^{-3}$
$\nabla c_k^{\delta_R/M} = 0$	None for $I \geq 2$ mA/cm^2

IV. CONCLUSIONS

A modified version of the BV model has been developed to describe the behavior of a membrane electrode assembly of a PEMFC. The model is based on "a posteriori" observation on the concentration profiles obtained from the BV model. Such an observation suggests that, from a very low value of the cell current density, the electrode bulk electrochemical reactions become surface electrochemical reactions occurring at the interface between the diffusive and reactive regions of the electrodes. Consequently, the Butler-Volmer equations have been analytically integrated in the reactive regions, and electro-kinetic expressions for the anode and cathode overpotentials have been obtained. A full new model, the MBV model, is constructed by inserting these electro-kinetic expressions into the mass and charge transport scheme developed in the Bernardi-Verbrugge work [2].

It turns out that the new model, as compared to the BV model, is *(i)* more stable from the numerical point of view, *(ii)* less sensible to trial input solution functions, and *(iii)* computationally faster (up to three order of magnitude). At high cell current densities, the new model is free from the severe numerical inaccuracies and instabilities induced by the non-linear nature of the Butler-Volmer equations, and it allows the finding of solutions over an extended range of cell current densities.

Since this work has been motivated by the negative consideration that the BV model (with all its numerical drawbacks), cannot be easily extended to treat 2D and 3D cases, we think to stay now, with the MBV model, to a stage of development in which these extensions could be performed. Work in this direction is in progress.

Our integration of the Butler-Volmer equations and, more precisely, the analytical expressions of the surface electrochemistry are making more explicit the role of the chemical species concentrations and of the cell current density on the performance curves. From the way in which these relations have been obtained, we are learning how to generalize the integration scheme in order to get a proper description of the concentration overpotentials at high cell current densities. Further work is in progress in this direction, too.

In addition, the integrated Butler-Volmer equations are also allowing us to make clear interpretations of the fitting parameters appearing in many "zero-dimensional", or empirical equation schemes, such those of Kim et al. [19] and of Squadrito et al. [20].

ACKNOWLEDGMENTS

This work has been carried out partially with the financial contribution of the Sardinia Regional Authorities, and partially with the financial support of the Centro Ricerche Fiat, Orbassano, Italy. Centro Ricerche Fiat is also acknowledged for the permission to publish some of the presented results, since they are based on a code developed by us and owned by them.

APPENDIX A: INTEGRATION OF THE BUTLER-VOLMER EQUATION

By applying the Butler-Volmer equations (16), (17) to the reactions (12) and (15), and by supposing an uniform proton concentration [2], we get

$$\nabla i^{\delta} = j^{\delta} = a i^{\delta}_{0,ref} \left(\frac{c_k}{c_{k,ref}} \right)^{\gamma_k} \left[e^{\alpha^{\delta}_a \beta_F (\Phi_s - \Phi)} - e^{-\alpha^{\delta}_c \beta_F (\Phi_s - \Phi)} \right] \quad \text{for } \delta = \text{A, C} \quad , \tag{A1}$$

where k stays for O_2 in C_R and for H_2 in A_R.

Since the only variations of the potentials inside the thin regions δ_R are of ohmic origin, as a first approximation we assume

$$\nabla(\Phi_s - \Phi) = 0 \quad , \tag{A2}$$

and we rewrite the Butler Volmer equations as

$$\nabla i^{\delta} = K^{\delta} c_k^{\gamma_k} \quad , \tag{A3}$$

where K^{δ} is a constant term.

As a second approximation, we neglect the convection term $c_k v$ in the Nernst-Planck equation, eq. (2),

$$N_k = -D_k \nabla c_k \quad , \tag{A4}$$

and, by applying eq. (18) for material balance, we write the current density variation as

$$\nabla i^{\delta} = -\frac{n^{\delta}_k F}{s^{\delta}_k} D_k \nabla^2 c_k \quad . \tag{A5}$$

The comparison of expressions (A3) and (A5) gives the second order differential equation

$$\nabla^2 c_k \propto c_k^{\gamma_k} \quad . \tag{A6}$$

To integrate such equation, we introduce a third approximation. We suppose that the reactant flux at the δ_R/M interfaces are zero

$$\nabla c_k^{\delta_R/M} = 0 \quad . \tag{A7}$$

and by integrating eq. (A5) we obtain

$$\nabla c_k^{\delta_R/\delta_D} = \frac{s^{\delta}_k I}{n_k F D_k} \quad . \tag{A8}$$

By using this last equation, the differential equation (A6) can be analytically integrated in the regions δ_R. When $\gamma_k \neq 1$, the solution is

$$c_k(z) = c_k(0) \left(1 + \frac{1-\gamma_k}{2} \frac{s^{\delta}_k I}{n^{\delta}_k F D_k c_k(0)} z \right)^{\frac{2}{1-\gamma_k}} \quad . \tag{A9}$$

where the zero of the z coordinate is at δ_R/δ_D interfaces.

This expression for $c_k(z)$ is inserted into eq. (A3), and eq. (A3) is integrated. We get

$$I^2 = K^{\delta} \frac{2 n^{\delta}_k F D_k}{s^{\delta}_k (\gamma_k + 1)} \left(c_k^{\delta_R/\delta_D} \right)^{\gamma_k + 1} \quad . \tag{A10}$$

By rearranging this expression, and by writing explicitly the term K we obtain the final general relation

$$e^{\alpha^{\delta}_a \beta_F (\Phi_s - \Phi)} - e^{-\alpha^{\delta}_c \beta_F (\Phi_s - \Phi)} = \frac{c_{k,ref}^{\gamma_k}}{a i^{\delta}_{0,ref}} \frac{s^{\delta}_k (\gamma_k + 1)}{2 n^{\delta}_k F D_k} \frac{I^2}{\left(c_k^{\delta_R/\delta_D} \right)^{\gamma_k + 1}} \quad . \tag{A11}$$

The application of this relation to the cathode semi-reaction (15), which means $k = O_2$, $\delta = C$, is performed by neglecting the exponential term $\exp(\alpha^C_a \beta_F (\Phi_s - \Phi))$ (negligible anode semi-reaction). If we write the result in terms of the cathode overpotential, $\eta^C = \Phi_s - \Phi$, we get

$$\eta^C = -\frac{1}{\alpha^C_c \beta_F} \left\{ 2 \ln I - \ln\left(\frac{2 n^C F D_{O_2}}{s^C_{O_2} (\gamma_{O_2} + 1)} a i^C_{0\text{ref}} c_{O_{2\text{ref}}} \right) - (\gamma_{O_2} + 1) \ln\left(\frac{c_{O_2}^{C_D/C_R}}{c_{O_{2\text{ref}}}} \right) \right\} \quad , \tag{A12}$$

which is expression (23) of the text.

Instead, by choosing $k = H_2$, $\delta = A$ and by assuming $\alpha^A_a = \alpha^A_c$, relation (A11) gives

$$\eta^A = \Phi_s - \Phi = \frac{1}{\alpha^A \beta_F} \ln\left(B + \sqrt{B^2 + 1} \right) \quad , \tag{A13}$$

with

$$B = \frac{s^A_{H_2} I^2 c_{H_{2\text{ref}}}^{\gamma_{H_2}} (\gamma_{H_2} + 1)}{2 n^A F \; a \; i^A_{0\text{ref}} \left(c_{H_2}^{A_D/A_R} \right)^{\gamma_{H_2}+1} D_{H_2}} \quad , \tag{A14}$$

which is expression (22) of the text. However, the assumption on the equality of the α^A_i values can be released but, in this case, the analytical solution is lost and a numerical inversion of eq. (A11) has to be performed.

LIST OF SYMBOLS

a	effective catalyst area per unit volume
$\mathrm{A_D}$	anode diffusion region
$\mathrm{A_F}$	anode flow region
$\mathrm{A_R}$	anode reaction region
c_i	concentration of species i
$\mathrm{C_D}$	cathode diffusion region
$\mathrm{C_F}$	cathode flow region
$\mathrm{C_R}$	cathode reaction region
D_i	diffusion coefficient of species i
D_{ij}	diffusion coefficient of the pair ij in a gas binary mixture
F	Faraday constant
$\mathbf{i}$	ionic current density
$\mathbf{i}_s$	electronic current density
i_0^β	exchange current density at the electrode β
$\mathbf{I}$	cell current density
j^β	Butler-Volmer current density source term in electrode β
k_p	hydraulic permeability
k_Φ	electrokinetic permeability
$\mathbf{N}_i$	mass flux of species i
K_i	Henry's law constant of species i
M	membrane region
n^β	number of electrons of the rate determining step at the electrode β
P	hydraulic pressure
R	gas constant
s_i^β	stoichiometric coefficient of species i reacting at the electrode β
T	temperature
$\mathbf{v}$	water velocity in pores
$\mathbf{v}_s$	water velocity through a planar surface
x_i	molar fraction of species i
y_i	mass source term of species i
z	distance
z_i	valence of species i

Greek symbols

α_a^β	anode transfer coefficient at the electrode β
α_c^β	cathode transfer coefficient at the electrode β
β_F	Faraday constant in units of RT
γ_i	kinetic exponent of the species i in the Butler-Volmer equation
ε_α^β	volume fraction of phase α in region β
ζ	O_2 stoichiometric inlet flow
κ	ionic conductivity
μ	pore-fluid viscosity
ρ	water density
σ	electronic conductivity
Φ	electric potential of the liquid phase
Φ_s	electric potential of the solid phase

Subscripts and superscripts

$*$	effective in porous media
f	membrane fixed charge
ref	at the reference state
sat	saturation condition
w	water

REFERENCES

[1] D. M. Bernardi and M. Verbrugge, AIChE Journal **37**, 1151 (1991).

[2] D. M. Bernardi and M. Verbrugge, J. Electrochem. Soc. **139**, 2477 (1992).

[3] T. Springer, T. Zawodzinski, and S. Gottesfeld, J. Electrochem. Soc. **138**, 2334 (1991), lANL model.

[4] T. Springer, M. Wilson, and S. Gottesfeld, J. Electrochem. Soc. **140**, 3513 (1993).

[5] V. Gurau, H. Liu, and S. Kakac, AIChE J. **44**, 2410 (1998).

[6] A. Kulikovsky, J. Divisek, and A. Kornyshev, J. Electrochem. Soc. **146**, 3981 (1999).

[7] S. Um, C.-Y. Wang, and K. Chen, J. Electrochem. Soc. **147**, 4485 (2000).

[8] J. Divisek, J. Mosing, B. Steffen, and U. Stimming, in *Electrochemical Engineering and Energy*, edited by F. Lapicque (Plenum Press, New York, 1995).

[9] S. Gottesfeld and T. Zawodzinski, in *Advances in Electrochemical Science and Engineering*, edited by R. Alkire, H. Gerischer, D. Kolb, and C. Tobias (Wiley, Weinheim, 1998).

[10] V. Gurau, Ph.D. thesis, University of Miami, Coral Gables, Florida (1998).

[11] J. Newman, *Electrochemical Systems* (Prentice-Hall, Englewood Cliff, NJ, 1973).

[12] R. Bird, W. Stewart, and E. Lightfoot, *Transport Phenomena* (John Wiley & Sons, Inc., New York, 1960).

[13] R. Schlögl, Z. Physik. Chem. **3**, 73 (1955).

[14] R. Schlögl, Ber. Bunsenges. Phys. Chem. **70**, 400 (1966).

[15] M. Verbrugge and R. Hill, J. Electrochem. Soc. **137**, 886 (1990).

[16] J. Bockris and A. Reddy, *Modern Electrochemistry* (Plenum, New York, 1970).

[17] H. Versteeg and W. Malalasekera, *An introduction to computational fluid dynamics. The finite volume method* (Longman Scientific & Technical, Harlow, 1995).

[18] J. Fiard and R. Herbin, Comput. Methods Appl. Mech. Eng. **115**, 315 (1994).

[19] J. Kim, S. Lee, S. Srinivasan, and C. Chamberlin, J. Electrochem. Soc. **142**, 2670 (1995).

[20] G. Squadrito, G. Maggio, E. Passalacqua, F. Lufrano, and A. Patti, J. Appl. Electrochem. **29**, 1449 (1999).